Experimental and Computational Studies of Structure and Bonding in Parent and Reduced Forms of the Azo Dye Orange II

Laurence C. Abbott,[†] Stephen N. Batchelor,[‡] John Oakes,[‡] Bruce C. Gilbert,[†] Adrian C. Whitwood,[†] John R. Lindsay Smith,[†] and John N. Moore*[,†]

Department of Chemistry, The University of York, Heslington, York YO10 5DD, U.K., and Unilever Research, Port Sunlight, Quarry Road East, Bebington, Wirral CH63 3JW, U.K.

Received: October 20, 2004; In Final Form: December 13, 2004

The structure and bonding of the azo dye Orange II (Acid Orange 7) in parent and reduced forms have been studied using NMR, infrared, Raman, UV−visible, and electron paramagnetic resonance (EPR) spectroscopy, allied with density functional theory (DFT) calculations on three hydrazone models (no sulfonate, anionic sulfonate, and protonated sulfonate) and one azo model (protonated sulfonate). The calculated structures of the three hydrazone models are similar to each other and that of the model without a sulfonate group (Solvent Yellow 14) closely matches its reported crystal structure. The ^{1}H and ^{13}C NMR resonances of Orange II, assigned directly from 1D and 2D experimental data, indicate that it is present as ≥95% hydrazone in aqueous solution, and as a ca. 70:30 hydrazone:azo mixture in dimethyl sulfoxide at 300 K. Overall, the experimental data from Orange II are matched well by calculations on the hydrazone model with a protonated sulfonate group; the IR, Raman, and UV−visible spectra of Orange II are assigned to specific vibrational modes and electronic transitions calculated for this model. The EPR spectrum obtained on one-electron reduction of Orange II by the 2-hydroxy-2-propyl radical (•CMe_2OH) at pH 4 is attributed to the hydrazyl radical produced on protonation of the radical anion. Calculations on reduced forms of the model dyes support this assignment, with electron spin density on the two nitrogen atoms and the naphthyl ring; in addition, they provide estimates of the structures, vibrational spectra, and electronic transitions of the radicals.

Introduction

Azo dyes are widely used in the textile, paper, food, cosmetic, and pharmaceutical industries,[1] and there is a need to understand and control their degradation reactions. Two contrasting situations are important: limited degradation is required while the dyes act as colorants, whereas efficient degradation is required for their disposal. Various degradation mechanisms have been proposed, depending on the conditions, and dye radicals are implicated as primary intermediates along many of the proposed reaction pathways.

Dye radical formation can be induced directly, by photochemical or electrochemical means, or by chemical or biological agents which reduce or oxidize the dye. Oxidation has been widely studied because it is implicated in dye degradation by chemical agents such as hypochlorite,[2] hydrogen peroxide,[3] and peracids.[4] Reduction has received less attention, but it is also important because it produces aromatic amines, some of which are known carcinogens, and it can be induced by biological agents such as liver enzymes, intestinal flora, and aquatic and skin bacteria; there is also interest in the use of bacterial reduction as an inexpensive method for the efficient degradation of dye effluent.[5−9] In another context, UV irradiation of cellulose produces polysaccharide free radicals,[10−12] including α-hydroxy radicals which are effective reducing agents[13] that can cause the undesirable degradation of azo dyes on cotton or paper. Hence, there is a need to understand the routes by which azo dyes are reduced, both as the free dyes and when bound to surfaces.

A good understanding of the structure and bonding of a parent azo dye is a prerequisite for characterizing its reactive radical intermediates. Crystal structures of several azo dyes have been reported,[14−19] and there have been many spectroscopic studies, but much remains to be learned about the structure and bonding of azo dyes and how they are influenced by the surrounding molecular environment.[20] Azo dyes containing a hydroxyl group which is ortho or para to the azo group within naphthyl or higher fused ring systems can exist as azo and hydrazone tautomers,[1] with the relative amounts varying with external parameters such as solvent and temperature. The presence of these two species can complicate the assignment of spectra because there may be bands from both species, as in the case of UV−visible and vibrational spectroscopies, or there may be an average band dependent on the composition, as in the case of NMR spectroscopy[21,22] because the equilibrium is fast on the NMR time scale. An additional complication may arise from aggregation, which occurs for many azo dyes in aqueous solution,[23] because the presence of dimers and higher aggregates can have a marked effect on the observed spectra, particularly UV−visible and NMR spectra.[24−26] Tautomerism and aggregation may both occur for a single dye, giving a multicomponent mixture with complex spectra. In addition, recent advances in theoretical techniques now enable the structure and spectroscopy of azo[27−36] and other dyes[37,38] to be studied to a high level by computational chemistry.

Direct studies of azo dye radicals have been relatively limited, with these reactive intermediates generally being investigated by flash photolysis,[39−41] pulse radiolysis,[39,42−49] and matrix isolation[44] methods using UV−visible absorption detection.

[†] The University of York.
[‡] Unilever Research.

10.1021/jp045216s CCC: $30.25
Published on Web 02/24/2005

Recent pulse radiolysis studies[42,43] followed the formation and decay of radicals from a range of small azo dyes and provided detailed information on the mechanisms and kinetics of reduction and oxidation processes. The EPR spectra obtained on reduction of some azo dyes have given an insight into the nature of the dye radicals.[10,50] However, there remains a need for the application of techniques which can provide detailed information on how the structure and bonding within azo dyes change on radical formation.

In this paper, we report an experimental and computational study of the simple azo dye Orange II (Acid Orange 7) and the radicals obtained on one-electron reduction (Scheme 1). Orange II has been studied widely, and it is reported to exist mainly as the hydrazone form in aqueous solution[2] and for dimers to dominate at concentrations above ca. 10^{-3} mol dm^{-3}.[24,26] We have studied the parent dye using NMR, infrared, Raman, and UV−visible spectroscopy, recording spectra under conditions where the dye monomer is dominant, where practicable. The experimental results have been allied with those from density functional theory (DFT) calculations on three hydrazone tautomers, **1** (Solvent Yellow 14), **2**, and **3**, containing no sulfonate group, a negatively charged SO_3^- group, and an SO_3H group, respectively, and the azo tautomer, **3-azo**; all of these dyes act as models for Orange II. We have used EPR spectroscopy to study the species obtained on one-electron reduction of Orange II by the 2-hydroxy-2-propyl radical, allied with DFT calculations on the radical anions, **3**$^{\bullet-}$ and **3-azo**$^{\bullet-}$, and on the neutral radical **3H**$^{\bullet}$ formed by protonation of either tautomer (Scheme 1). This combination of experimental and computational techniques has enabled us to study both parent and reduced forms of Orange II at a high level of detail, providing important evidence on how the structure and bonding change on radical formation.

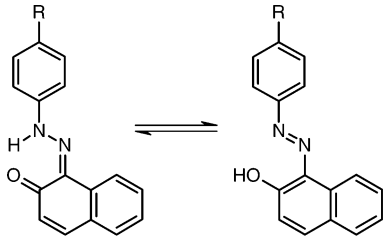

Orange II: R = SO_3Na

1: R = H	**1-azo**: R = H
2: R = SO_3^-	**2-azo**: R = SO_3^-
3: R = SO_3H	**3-azo**: R = SO_3H

Experimental Section

Experimental Methods. Orange II (Sigma) was purified;[2] oven-dried KBr (Aldrich, FT-IR grade), H_2O_2 (Fisher Scientific), propan-2-ol (Fisher Scientific), $TiCl_3$ (10 wt % in 20−30 wt % HCl, Aldrich), D_2O, dimethyl sulfoxide-d_6 (DMSO-d_6) (Goss Scientific), and freshly deionized water were used as received. 1D and 2D ^1H and ^{13}C NMR spectra were recorded at 300 K using a Bruker AMX-500 spectrometer; spectra were calibrated against residual protiated solvent resonances and were processed using XWIN NMR (Bruker). UV−visible spectra were recorded using a Hitachi U-3010 spectrophotometer, and infrared spectra were recorded using a Nicolet Impact 410 FTIR spectrometer. Resonance Raman scattering was excited using either the 647.1, 568.2, or 406.7 nm line from a Kr^+ laser (Coherent Innova-90), collected at 90° to the incident beam, dispersed using a Spex 1403 double monochromator, and detected using a liquid nitrogen cooled CCD detector (Wright Instruments, Ltd.) at ca. 5 cm^{-1} resolution and ca. ±2 and ±4 cm^{-1} accuracy, for red and blue excitation, respectively. Samples were held in a spinning quartz cell; laser powers were typically 30 mW, and total collection times were typically 15 min, comprising several readouts. The sample integrity following Raman data collection was confirmed by UV−visible spectroscopy. Resonance Raman spectra were calibrated against solvent band positions and were base-line corrected using Grams/32 software (Galactic Industries Corp.). EPR spectra were recorded using a Bruker ESP300 X-band EPR spectrometer with 100 kHz modulation. Spectra were manipulated using WinEPR (Bruker), and simulated spectra were generated using Winsim from the Public EPR Software Tools package.[51] The reduced dye species were generated by reaction of Orange II with 2-hydroxy-2-propyl radicals[52−54] using a continuous flow system, and the electron paramagnetic resonance (EPR) spectrum was obtained from averaging 142 scans taken over 7 h total acquisition time. A three-way mixing system was employed, the flow being maintained by a peristaltic pump (Watson-Marlow 502s) positioned on the inlet tubes. The delay time between mixing and passage through the quartz flat cell (0.26-cm path length) placed in the EPR cavity was ca. 40 ms. The three aqueous streams contained $TiCl_3$ (5×10^{-3} mol dm^{-3}), H_2O_2 (3.4×10^{-2} mol dm^{-3}), and Orange II/propan-2-ol (1×10^{-3} mol dm^{-3}/1 mol dm^{-3}) (concentrations before mixing); the $TiCl_3$ solution was prepared at ca. pH 4, using concentrated sulfuric acid, to inhibit its hydrolysis/oxidation. All solutions were deoxygenated both prior to and during use by purging with oxygen-free nitrogen gas.

Computational Methods. All semiempirical and ab initio calculations were performed on isolated molecules using the Gaussian 98 package[55] on an Intel Pentium III-based PC running Linux, except for the time-dependent DFT (TD-DFT) calculations which were performed using the Gaussian 03 package[56] on a 20-processor Sun Microsystems Fire 6800. Starting geometries were optimized initially using the Dreiding molecular mechanics method[57] before using the B3LYP DFT functional[58] in conjunction with the 6-31G(d) basis set, and these optimized structures were used for further calculations. NMR shifts were calculated using the GIAO method[59] with the B3LYP functional and the 6-31G(d) basis set, and values are reported relative to tetramethylsilane (TMS) calculated at the same level of theory. Vibrational wavenumbers were calculated using the B3LYP functional and the 6-31G(d) basis set, and the values reported have been scaled by a factor of 0.9614;[60] calculated IR and Raman spectra were created by applying a 10 cm^{-1} full width at half-maximum (fwhm) Gaussian function scaled to the calculated intensity of each vibration, and then the entire spectra were scaled for comparison with the experimental data. Excited-state properties were calculated using both the ZINDO CIS method[61] and the PBE1PBE TD-DFT method[62] with the 6-31G-(d) basis set. EPR properties were calculated using the B3LYP functional and either the EPR-II[63] or 6-31G(d) basis sets, as outlined in the text. Output files from calculations were parsed and analyzed using software written in-house, and the Molekel (Version 4.3)[64] and Molden (Version 4.0) [65] packages.

Results and Discussion

Preface. Experimental and computational results from the parent dyes are presented first, followed by those from the reduced dyes. The calculated geometries of **1**−**3** were quite similar to each other, but the calculated spectral properties of **2** were very different from those of **1** and **3**, and from the

SCHEME 1: Parent and Reduced Dye 3 Species along with General Atom Numbering

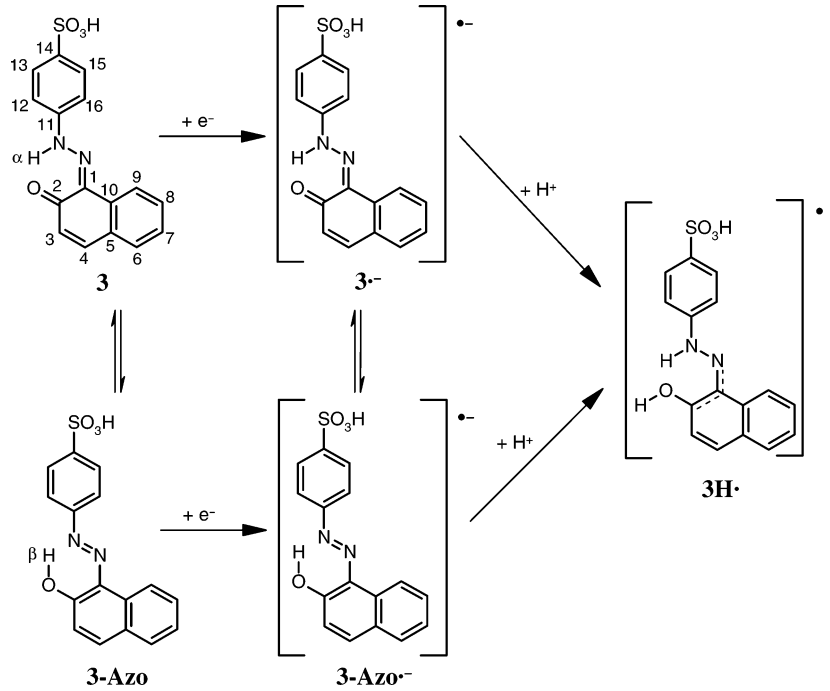

TABLE 1: Selected Bond Lengths (Å) and Angles (deg) for Parent and Reduced Dye Species Calculated at the B3LYP/6-31G(d) Level and Experimental Literature Values for Comparison

	parent dye					reduced dye		
	calculated			X-ray diffraction		calculated		
param	**1**	**3**	**3-azo**	**1**[a]	Orange G[b]	**3**•−	**3-azo**•−	**3H**•
				Bond Lengths				
$C_{11}-N_{11}$	1.401	1.394	1.410	1.406	1.405−1.412	1.355	1.361	1.384
$N_{11}-N_1$	1.308	1.315	1.280	1.308	1.290−1.303	1.356	1.342	1.337
N_1-C_1	1.328	1.323	1.378	1.338	1.339−1.350	1.352	1.365	1.355
C_1-C_2	1.477	1.482	1.419	1.457	1.459−1.461	1.463	1.429	1.420
C_1-C_{10}	1.466	1.468	1.448	1.453	1.447−1.462	1.455	1.453	1.461
C_2-O_2	1.255	1.252	1.332	1.261	1.262−1.270	1.283	1.349	1.381
$N_{11}-H_\alpha$	1.034	1.033				1.044		1.017
O_2-H_β			1.006				1.021	0.970
$O_2\cdots H_\alpha$	1.725	1.726				1.655		1.873
$N_{11}\cdots H_\beta$			1.663				1.607	
				Angles				
$C_{11}-N_{11}-N_1$	121.8	121.4	115.8	118.9	121.0−121.9	121.6	115.7	121.2
$N_{11}-N_1-C_1$	119.9	119.9	117.3	118.4	118.2−118.9	115.6	115.3	120.1
$N_1-C_1-C_2$	123.1	123.2	123.9	123.9	122.1−122.7	124.7	125.4	128.0
$C_1-C_2-O_2$	121.9	121.7	122.3	121.6	120.4−121.9	122.9	121.6	118.5
$H_\alpha-N_{11}-N_1$	116.6	116.6				114.7		120.1
$H_\beta-O_2-C_2$			106.3				104.2	109.3

[a] Reference 14. [b] Reference 15 (ranges given for structures with NH_4^+, Li^+, Mg^{2+}, and Ca^{2+} counterions).

experimental spectra of Orange II. The calculations on **3** gave the best match with the experimental results from Orange II; although the sulfonate group of Orange II was not protonated under the conditions used, the calculations on **3** evidently provide the best model for its hydrated form. Consequently, the paper generally focuses on comparisons of the experimental data with the calculated results from **3** and **3-azo**, with the results from calculations on **1** and **2** included where important; complete results from all the calculations are included in the Supporting Information.

Parent Dyes. The optimized geometries from our DFT calculations on **1**−**3** are considered first and discussed in the context of reported dye structures. Our experimental NMR, IR, Raman, and UV−visible results on Orange II are then presented and discussed in comparison with values calculated from these optimized geometries.

Geometry Optimizations. The calculated geometries of **1**−**3** and **3-azo** were optimized using the B3LYP DFT functional with the 6-31G(d) basis set: Figure 1 shows the optimized geometry of **3**. Table 1 lists selected bond lengths and angles calculated for **1**, **3**, and **3-azo**, along with parameters reported from X-ray diffraction studies of **1**[14] and Orange G with various counterions,[15] both of which were observed to be in the hydrazone form. In each case calculated here, the optimized

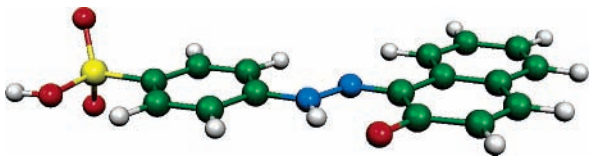

Figure 1. Optimized structure of **3** determined at the B3LYP/6-31G-(d) level.

TABLE 2: Experimental ^{1}H and ^{13}C NMR Shifts (ppm) and Assignments of Orange II and Calculated Shifts of 3 and 3-azo

	experimental: Orange II				calculated			
	D_2O		DMSO-d_6		**3**		**3-azo**	
atom	H[a]	C	H[a]	C	H	C	H	C
1		129.1		129.4		127.1		126.1
2		178.4		169.9		172.8		148.9
3	5.59 1, d	124.3	6.88 1, d	124.2	6.40	121.6	6.98	113.5
4	6.73 1, d	143.2	7.93 1, d	140.2	7.30	137.2	7.65	133.4
5		127.2		127.8		122.2		121.3
6	6.71 1, d	128.7	7.75 1, d	128.9	7.19	123.6	7.54	123.1
7	6.50 1, t br	126.4	7.44 1, t	125.9	7.22	120.2	7.40	118.5
8	6.42 1, t br	128.7	7.60 1, t	129.1	7.39	123.4	7.60	123.0
9	7.06 1, d	120.5	8.52 1, d	121.4	8.26	117.0	8.75	116.2
10		131.7		132.7		128.3		127.9
11		142.2		147.3		137.6		145.7
12/16	6.29 2, d	115.6	7.77 2, d	118.1	7.30	109.0	7.79	115.6
13/15	7.11 2, d	126.4	7.81 2, d	127.1	7.63	120.8	7.75	120.2
14		139.0		144.8		133.5		137.6
H_α			15.82 1, s		14.66			
H_β							13.61	

[a] Integration, multiplicity (d = doublet; t = triplet; br = broad).

geometry is planar, with a dihedral angle of 180.0° about the hydrazone or azo group, $C_1-N_1-N_{11}-C_{11}$ (Scheme 1), and the $O_2\cdots H_\alpha$ distance is significantly less than the sum of the van der Waals radii (2.6 Å), showing the presence of a hydrogen bond. A direct comparison between calculated and reported[14] experimental structures is available only for **1**, and the agreement is good: most calculated bond lengths are within <1% of those in the crystal structure, with the largest difference being a calculated C_1-C_2 bond length of 1.477 Å, which is 0.02 Å longer than that in the crystal. This good agreement gives confidence in the results of the other calculations, where experimental structures are not available for comparison.

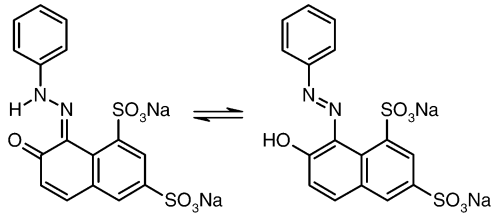

Orange G

The calculated structures of **1**−**3** show relatively small differences between each other (Table S1). On adding an SO_3^- group to **1** to give **2**, the C_1-C_2 bond shortens, the N_1-C_1 bond lengthens, and the N_1-N_{11} bond shortens; other bond lengths change by <0.5%. Protonation of the SO_3^- group of **2**, to give **3**, reverses these changes, and, consequently, the calculated bond lengths of **3** are generally within <0.5% of those of **1**. The changes in the calculated bond angles show a similar trend, such that the calculated structures of **1** and **3** are very similar overall: the calculations indicate that the addition of an SO_3H group does not significantly affect the structure and bonding of the dye. A comparison of the experimental crystal structures reported for **1**[14] and Orange G[15] reveals that the addition of two SO_3Na groups to the naphthyl ring causes only small changes in the bond lengths, similar to the small effect calculated here for **1** and **3**.

A comparison of the calculated geometries of **3** and **3-azo** indicates that the N−N bond shortens from 1.315 to 1.280 Å, the C_2-O_2 bond lengthens from 1.252 to 1.332 Å, the C_1-C_2 bond shortens from 1.482 to 1.419 Å, and the C_1-C_{10} bond shortens from 1.468 to 1.448 Å; these large changes are consistent with those expected between hydrazone and azo tautomers, including increased aromaticity in the azo form. The calculations indicate that other parts of the molecule are relatively unaffected by a change between tautomers, with bond length changes generally being <1%. The optimized geometry of **3** was calculated to be ca. 13.2 kJ mol^{-1} lower in energy than that of **3-azo**.

NMR Spectroscopy. Experimental NMR resonances from Orange II in D_2O and DMSO-d_6 solution are listed in Table 2 along with assignments made using a combination of COSY and short-range and long-range HMQC spectra; they are consistent with the literature.[26] Most of the ^{13}C resonances show small (<5 ppm) changes between D_2O and DMSO-d_6 solutions; the largest change occurs for the resonance from C_2, which shifts from 178.4 to 169.9 ppm on going from D_2O to DMSO-d_6 and is attributed to a shift in the azo−hydrazone equilibrium. Experimental studies of similar azo dyes[21,25] give a ^{13}C resonance for C_2 at ca. 179−180 ppm for a pure hydrazone dye and at ca. 154−156 ppm for a pure azo dye, with an azo−hydrazone mixture giving a resonance proportionately between these two limits, depending on the relative amounts of the two tautomers. Therefore, the C_2 resonance from Orange II indicates that it is present as ≥95% hydrazone in D_2O and as a ca. 70:30 hydrazone:azo mixture in DMSO-d_6; the observation that the hydrazone is more stable than the azo tautomer is consistent with the relative calculated energies of the isolated molecules. The downfield position of the H_α resonance of Orange II in DMSO-d_6 indicates that there is hydrogen bonding with O_2, consistent with the calculated geometries (Table 1). The ^{1}H resonances show stronger shifts than the ^{13}C resonances on going from D_2O to DMSO-d_6, with most ^{1}H resonances shifting downfield by >1 ppm; the H_α resonance is absent in D_2O, showing that this proton undergoes deuterium exchange. At the concentration used to record the NMR spectrum in D_2O (9×10^{-2} mol dm^{-3}), Orange II is predominantly present as dimers (<10% monomer).[24,26] The ^{1}H resonances of azo dyes, including Orange II, have been reported to shift upfield with increasing concentration in D_2O,[26,66] due to π-stacking, whereas the ^{13}C resonances are relatively unaffected. By contrast, Orange II does not aggregate in DMSO,[3] and we attribute the major differences in the ^{1}H resonances observed here between D_2O and DMSO-d_6 solutions to aggregation effects, although more specific solvation effects may also occur.

The calculated resonances of **3** and **3-azo** were determined at the B3LYP/6-31G(d) level and are given in Table 2 alongside

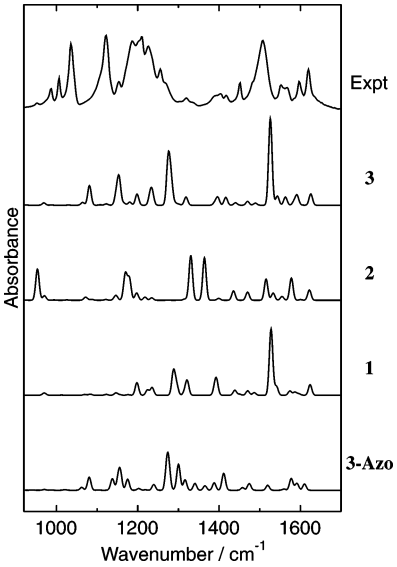

Figure 2. Experimental infrared spectrum of Orange II in KBr and infrared spectra of **1**−**3** and **3-azo** calculated at the B3LYP/6-31G(d) level.

the experimental values; the calculated resonances for all the dyes are given in Table S2. The calculated ^{1}H chemical shifts for both **3** and **3-azo** show the general trends observed in the experimental data: the resonance of H_α or H_β is much further downfield than those of the other protons, H_9 is next furthest downfield, H_3 is furthest upfield, and the remainder are relatively close together. The calculated ^{1}H resonances of **3-azo** are all slightly downfield from those of **3**. The calculated ^{13}C resonances of **3** are generally within ca. 5 ppm of the experimental values for Orange II in DMSO-d_6, with the largest differences being for carbons within the phenyl ring; these differences may arise from the effects of the nearby sulfonate group, which is protonated in the calculations and is a solvated anion in solution. The largest difference between the calculated ^{13}C resonances of **3** and **3-azo** is for C_2, as would be expected for the hydrazone and azo tautomers: it is calculated at 172.8 ppm for **3** and 148.9 ppm for **3-azo** (Table 2), both ca. 7 ppm lower than the reported experimental values for pure hydrazone and azo tautomers.[21,25] The match between the experimental and calculated chemical shifts is not perfect but the situation here is complicated by the presence of aggregation effects in D_2O and a tautomeric mixture in DMSO-d_6. Nonetheless, NMR calculations can assist with the assignment of NMR spectra and may be particularly helpful if 2D NMR data are not available.

Vibrational Spectroscopy. Figure 2 shows the experimental infrared spectrum of Orange II in a KBr pellet along with calculated infrared spectra of **1**−**3** and **3-azo**. Figure 3 shows experimental Raman spectra of Orange II in aqueous solution recorded with excitation wavelengths of 647.1 (off resonance), 568.2, and 406.7 nm (on resonance) (Figure 4) along with calculated Raman spectra of **1**−**3** and **3-azo**. Table 3 lists experimental band positions along with calculated wavenumbers, infrared and Raman intensities, and mode descriptions for selected modes of **3**; calculated values for all of the dyes are given in the Supporting Information. Orange II is present as ca. 90% monomer at the concentration used to record the Raman spectra (1×10^{-4} mol dm^{-3}),[24,26] and our work on other azo dyes[66] has shown that their resonance Raman spectra in the ca. 1000−1700 cm^{-1} region are not affected significantly by π-stacking, in which the internal structure of the individual dye molecules is largely retained. Thus, the observed spectra effectively characterize the monomer dye.

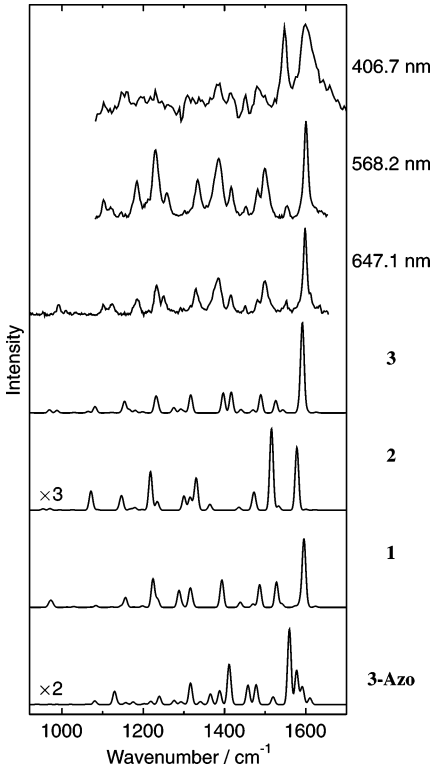

Figure 3. Experimental Raman spectra of Orange II at 1×10^{-4} mol dm^{-3} in aqueous solution recorded with 406.7, 568.2, and 647.1 nm excitation wavelengths, and Raman spectra of **1**−**3** and **3-azo** calculated at the B3LYP/6-31G(d) level.

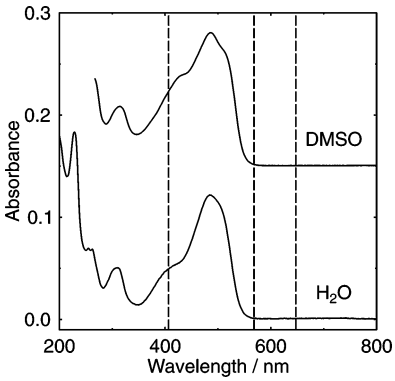

Figure 4. Experimental UV−visible spectra of Orange II (ca. 8×10^{-6} mol dm^{-3}; 1 cm cell) in aqueous and DMSO solutions. The DMSO spectrum is offset for clarity, and dashed lines show excitation wavelengths used to record Raman spectra.

The calculated Raman spectrum of **3** at 1200−1700 cm^{-1} matches the experimental off-resonance spectrum of Orange II well, in terms of both band positions and intensities (Figure 3), and the assignment of these bands is relatively straightforward; Table 3 gives the major contributions, which may be compared with the simple group frequency assignments reported previously for Orange II.[67,68] The calculations show that the vibrational modes generally involve contributions from several parts of the molecule, rather than localized displacements, and figures of the displacement vectors for all the modes of **1**−**3** and **3-azo** are given in the Supporting Information (Figures S1−S4). Figure 5 shows the displacement vectors of calculated modes of **3** which are assigned to characteristic Raman bands of Orange II. The strongest Raman band at 1598 cm^{-1} is assigned to a calculated mode at 1592 cm^{-1} that involves Wilson 8a and 9a vibrations of the phenyl ring coupled to N−H bending; a strong Raman band at 1499 cm^{-1} is assigned to a calculated mode at

TABLE 3: Experimental Infrared and Raman Band Positions (cm^{-1}) of Orange II in the 950−1700 cm^{-1} Region with Assignments to Calculated Vibrational Modes of 3[a]

experimental: Orange II								calculated: **3**			
		Raman[b]							intensity[c]		
IR		647.1		568.2		406.7			IR	R	description[d]
1620	s	1622	w					1626	13	1	ν(CO), δ(NH), δ(naph)
1597	m	1598	vs	1600	vs	1597	vs	1592	11	100	ν(Ph) 8a, δ(Ph) 9a, δ(NH)
1584	w							1584	4	6	δ(NH), ν(CO), δ(naph)
1567	m							1563	9	0	ν(Ph) 8b, δ(Ph) 3, δ(NH), ν(NN), δ(naph)
1552	m	1552	w	1554	w	1548	vs	1543	11	3	δ(naph), δ(NH)
1507	vs	1510	sh					1526	100	14	δ(NH), δ(naph), ν(CN)
		1499	s	1499	s	1499	w	1489	2	20	ν(Ph) 19a, δ(Ph) 18a, ν(CN)
1483	sh	1481	w	1481	m	1481	s	1470	4	3	δ(naph), ν(NN)
1451	m	1451	w	1452	w	1451	m	1440	3	4	δ(naph)
1418	w	1416	m	1417	m	1416	m	1417	9	23	ν(Ph) 19b, δ(Ph) 18b, ν(CN), δ(NH), δ(naph)
1403	w										
1391	w	1385	s	1386	vs	1386	s	1397	9	22	ν(Ph) 19b, δ(Ph) 18b, δ(NH), ν(CN)
1335	w							1319	9	3	δ(naph), δ(Ph), ν(NN)
		1334	m	1334	s			1316	1	17	ν(Ph) 14, δ(Ph) 3, δ(naph), δ(NH), ν(NN)
1319	w							1301	1	2	ν(Ph) 14, δ(Ph) 3, δ(naph), ν(NN), δ(NH)
1302	w			1302	w			1292	2	4	ν(Ph) 8b, δ(Ph) 3, δ(naph)
1268	sh										
1256	s	1258	m	1258	m			1275	54	6	ν(NN), δ(NH), δ(naph), δ(Ph) 9a
		1250	m					1236	14	7	δ(naph)
1226	vs	1233	s	1230	s	1230	w	1230	11	15	ν(Ph), δ(Ph) 18a, δ(naph), ν(CN), δ(NH)
1210	vs	1210	w								
1202	sh										
1186	vs	1185	s	1184	s						
1153	m			1155	w	1155	w				
				1146	w						
1121	vs	1123	m	1121	w						
1106	sh	1102	m	1102	m						
1036	vs	1034	w								
1006	s	1009	w								
986	m	991	m								
952	w										

[a] Calculated wavenumbers have been scaled by 0.9614, as outlined in the text; vs = very strong; s = strong; m = medium; w = weak; sh = shoulder. [b] Excitation wavelength in nanometers. [c] Scaled to a maximum of 100. [d] Descriptions given in order of decreasing contribution; δ(naph) and δ(Ph) indicate a general distortion of a naphthyl or phenyl moieties, respectively, and associated numbers indicate Wilson vibrations.

1489 cm^{-1} involving Wilson 18a and 19a vibrations of the phenyl ring; and a moderately strong pair of Raman bands at 1416 and 1385 cm^{-1} is assigned to calculated modes at 1417 and 1397 cm^{-1} that involve Wilson 18b and 19b vibrations of the phenyl ring coupled with opposite phases to N−H bending and C−N stretching vibrations. The calculated IR spectrum of **3** at 1200−1700 cm^{-1} also matches the experimental spectrum of Orange II reasonably well, and the bands are assigned accordingly (Table 3). Strong bands from modes involving sulfonate vibrations occur in the 950−1200 cm^{-1} region,[67] but a direct assignment of the calculated modes of **3** (sulfonate protonated) to the experimental IR bands of solid Orange II (sulfonate bound to Na^+) and Raman bands of aqueous Orange II (sulfonate hydrated) cannot be made with confidence.

The good overall match between the experimental spectra and the calculated spectra of **3** gives further confidence in the calculated structure. The calculated vibrational spectra of **1** match the main features in the experimental spectra of Orange II relatively well, but they lack some bands, particularly in the ca. 950−1200 cm^{-1} region of the infrared spectrum where bands arising from sulfonate modes are expected. By contrast, the calculated vibrational spectra of **2** clearly are different from the experimental spectra, showing that the presence of a charged SO_3^- group provides a poor model for Orange II solvated by water: this effect may be relevant generally to calculations on sulfonated dyes. The calculated infrared and Raman spectra of **3-azo** also are very different from the experimental spectra of Orange II, consistent with the hydrazone tautomer being dominant in aqueous solution.[2]

Electronic Structure. The UV−visible spectra of Orange II in H_2O and DMSO are shown in Figure 4, recorded at concentrations (8×10^{-6} mol dm^{-3}) where the dye is >99% monomeric;[24,26] the band at 484 nm in H_2O ($\epsilon = 1.6 \times 10^4$ dm^3 mol^{-1} cm^{-1}) is responsible for the color. A shoulder at ca. 433 nm is present for the DMSO but not the aqueous solution and, by comparison with the solvent-dependent spectra reported for similar azo dyes,[69] it may be attributed to the azo tautomer; its presence arises from the shift in the azo−hydrazone equilibrium discussed above (NMR spectroscopy).

The lowest three electronic transitions of **3** and **3-azo** were calculated by both the PBE1PBE/6-31G(d) time-dependent DFT (TD-DFT) method[62] and the ZINDO semiempirical method,[61] and the calculated transition energies and oscillator strengths are tabulated in Table 4; the calculated values for all of the dyes are listed in Table S3. Additionally, the nature of the transitions calculated with the TD-DFT method were explored by examining the changes in electron density obtained by subtracting the ground-state electron density from the excited-state electron density, as shown for **3** and **3-azo** in Figure 6; the changes for all of the dyes are shown in Figure S5.

Qualitatively, the calculated transitions from the two different methods applied to **3** give similar results, comprising a disallowed carbonyl n $\rightarrow \pi^*$ transition ($f \approx 0$) as the lowest energy transition; a strong $\pi \rightarrow \pi^*$ transition ($f \approx 0.5$) in the visible region, which involves charge redistribution around the N−N and carbonyl groups, and the naphthyl ring; and a moderately strong $\pi \rightarrow \pi^*$ transition ($f \approx 0.2$) in the near-UV region, which involves charge transfer from the naphthyl ring onto the N−N

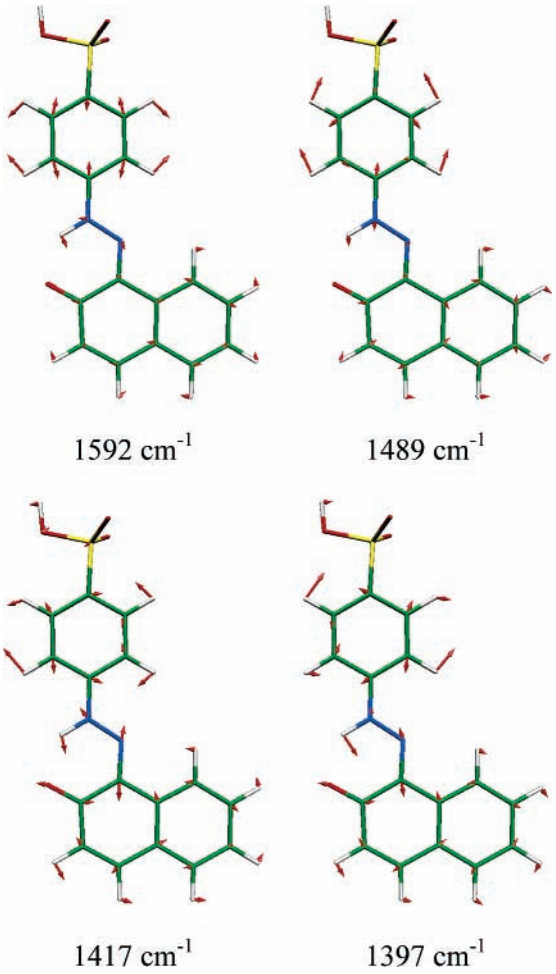

Figure 5. Calculated displacement vectors for vibrational modes of **3** assigned to strong experimental Raman bands of Orange II.

and carbonyl groups. The calculated energy of the strongest transition does not match the experimental energy particularly well: the TD-DFT method gives a slightly closer match, but the ZINDO method requires considerably less computing time.

The calculated transitions of **1** are similar to those of **3**, but the calculated transitions of **2** involve charge transfer from the electron-rich SO_3^- group onto the rest of the molecule; they are very different from those calculated for **1** and **3** (Figure S5), as are the calculated transition energies, oscillator strengths (Table S3), and changes in electron density. It is evident that an unsolvated SO_3^- group does not model the experimental data from Orange II well, again suggesting that calculations on dyes with charged SO_3^- groups may generally not give satisfactory results for comparison with data from solvated dyes.

Experimentally, the absorption peak from an azo tautomer generally is observed at higher energy than that from the hydrazone tautomer.[69] The strongest transitions of **3** and **3-azo** are calculated to be similar in energy by both the TD-DFT and ZINDO methods, with that of **3-azo** at slightly lower energy. The calculated changes in electron density for the lowest three transitions of **3-azo** show some similarities to those determined for **1** and **3**: that at lowest energy is a very weak azo n $\rightarrow \pi^*$ transition ($f \approx 0$), and the second and third transitions are stronger $\pi \rightarrow \pi^*$ transitions ($f > 0.08$). The nature of the strongest (second) transition is different from that of the hydrazone tautomer: for **3-azo**, it involves charge transfer from the naphthyl ring onto both nitrogen atoms of the azo group, and there is less charge redistribution within the naphthyl ring. These calculations are comparable with reported calculations on the azo and hydrazone tautomers of Orange II at the lower PPP level,[68] and also on azobenzene using DFT methods;[35,70,71] azobenzene is well-known to have a weak, low-energy n $\rightarrow \pi^*$ transition and a strong $\pi \rightarrow \pi^*$ transition.[72]

The calculations performed here were on isolated rather than solvated molecules. The electronic structures of azo dyes can be affected strongly by solvent, including the preferential stabilization of one tautomer over the other, and this may account for some of the differences between the calculated and experimental transition energies.

Reduced Dyes. Our experimental EPR study of Orange II is presented first, followed by the results of our DFT calculations on radicals, including optimized geometries and EPR, vibrational, and electronic parameters.

EPR Spectroscopy. Radicals were created by mixing aqueous $TiCl_3$, H_2O_2, and propan-2-ol solutions at pH 4, with the principal reactions given by (1) and (2).

$$Ti^{3+} + H_2O_2 \rightarrow Ti^{4+} + {}^{\bullet}OH + OH^- \quad (1)$$

$$CHMe_2OH + {}^{\bullet}OH \rightarrow {}^{\bullet}CMe_2OH + H_2O \quad (2)$$

EPR spectra recorded without Orange II present gave the characteristic spectrum of $^{\bullet}CMe_2OH$ (with traces of $^{\bullet}CH_2CHMeOH$).[52] Spectra recorded with Orange II present showed a dramatic decrease in the signal from the 2-hydroxy-2-propyl radical and the appearance of a new and complex signal, with multiple splittings, evidently resulting from the reaction of $^{\bullet}CMe_2OH$ with the dye.[73] Figure 7 shows the EPR spectrum of the dye radical, produced by a scaled subtraction of the signals in the absence of the dye from the spectrum obtained in its presence, along with an optimized simulation (optimized overlap of line positions between experiment and simulation) using two nitrogen hyperfine splittings of $a_N = 4.32$ and 3.45 G and six hydrogen splittings of $a_H = 3.82$, 3.45, 2.85, 1.65, 1.50, and 1.00 G; the g value was 2.0032. The Orange I radical anion is reported to protonate rapidly in aqueous solution, with a pK_A of 7.9 for the hydroxyl group,[42] and the Orange II radical anion is likely to behave similarly.

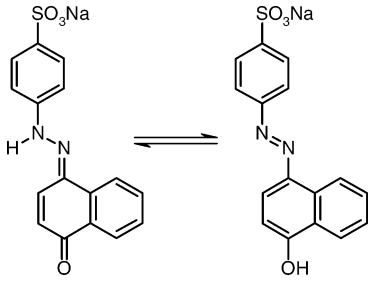

Orange I

Hence, we assign the observed EPR spectrum at pH 4 to that of the protonated radical anion of Orange II produced by reactions 3 and 4; this species is formed on protonation of either the hydrazone or azo tautomers of the reduced dye, as illustrated by Scheme 1.

$$dye + {}^{\bullet}CMe_2OH \rightarrow dye^{\bullet -} + Me_2CO + H^+ \quad (3)$$

$$dye^{\bullet -} + H^+ \rightarrow dyeH^{\bullet} \quad (4)$$

There have been relatively few reported EPR studies of azo species,[10,50,75−78] particularly of azo dyes.[10,50] One previous EPR

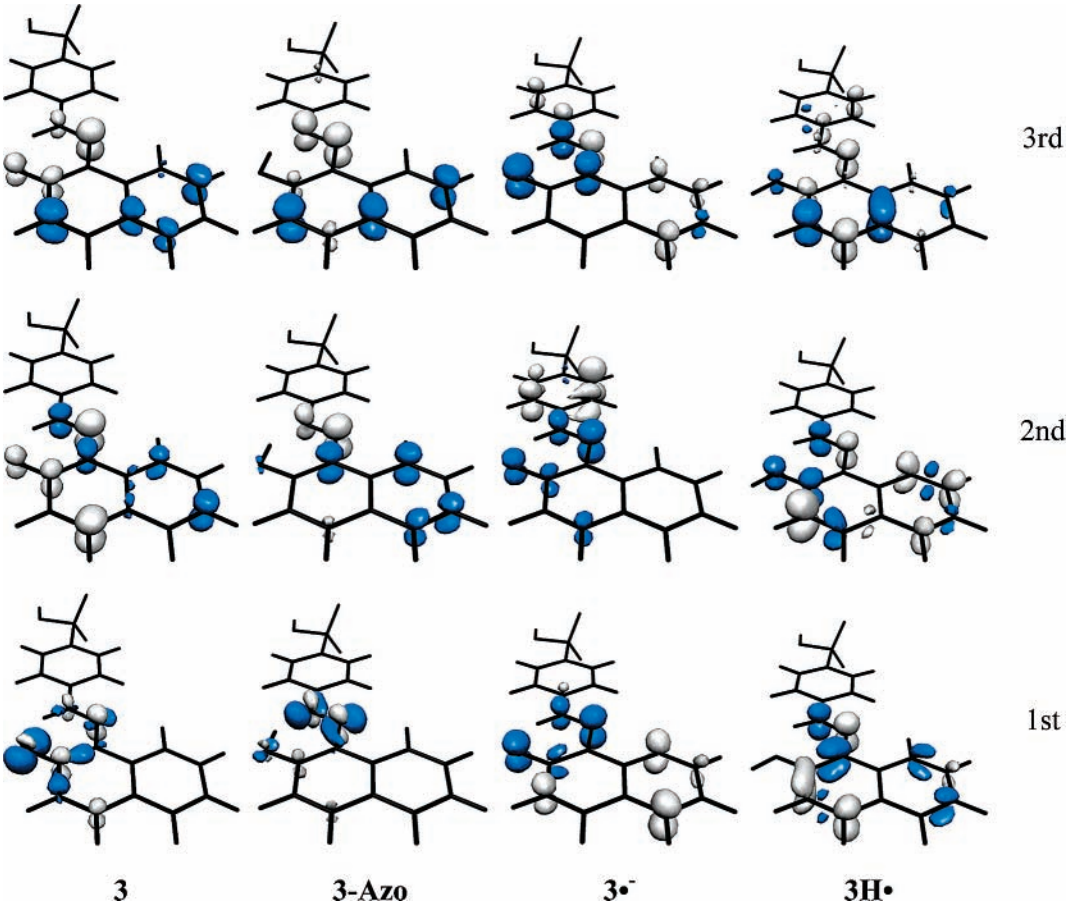

Figure 6. Calculated changes in electron density on excitation to the lowest three excited states of parent and reduced dye **3** species, determined using the PBE1PBE/6-31G(d) TD-DFT method. Blue and white regions represent a decrease and increase of electron density on excitation, respectively.

TABLE 4: Transition Energies and Oscillator Strengths (*f*) Calculated for the Lowest Three Singlet States of Dye 3 Species

	PBE1PBE/6-31G(d)			ZINDO		
species	energy/eV	λ/nm	*f*	energy/eV	λ/nm	*f*
3	2.86	434	0.0002	2.38	521	0.0001
	2.94	422	0.5333	3.00	413	0.5842
	3.31	375	0.1383	3.55	349	0.2545
3-azo	2.69	461	0.0000	2.38	521	0.0000
	2.90	427	0.5416	2.84	437	0.8835
	3.40	365	0.0837	3.53	351	0.1251
3$^{\bullet-}$	1.98	627	0.0288	2.08	597	0.0176
	2.31	537	0.0079	2.37	523	0.0020
	2.49	499	0.1302	2.47	502	0.1677
3H$^{\bullet}$	2.31	536	0.0290	2.88	430	0.0018
	2.92	425	0.2425	3.58	346	0.0013
	3.18	390	0.0428	3.62	343	0.0007

study of the reduction of several sulfonated 2-(naphthylazo)-1-naphthol dyes in ethanol[50] gave spectra that were simulated by two nitrogen splittings in the range of $a_N = 7.4-7.9$ and 4.5−5.7 G, three proton splittings of $a_H = 4.7-5.8$, 4.1−4.8, and 1.1−2.0 G, and $g = 2.0038$ for each dye; the observed spectra were assigned to protonated hydrazyl radical anions, as assigned here for Orange II. The splittings obtained here suggest that the electron spin densities on the nitrogen atoms in the protonated radical anion of Orange II in water are lower than the equivalent values for these other dyes in ethanol. EPR studies of the reduction of azobenzene[76,77] and substituted azobenzenes[78] in DMSO reported two identical nitrogen splittings of $a_N =$ 4.7−5.0 G, similar to the larger of the two nitrogen splittings determined here for Orange II; however, it is unlikely that these reduced azobenzene species were protonated under the reported conditions.

Geometry Optimizations. Optimized geometries of the reduced dyes, **1**$^{\bullet-}$, **2**$^{\bullet-}$, **3**$^{\bullet-}$, and **3-azo**$^{\bullet-}$, were calculated by taking the optimized geometries of the parent dyes, adding an electron, and optimizing at the B3LYP/6-31G(d) level. The optimized geometries of the reduced species were then protonated, at either O_2 or N_{11}, and further optimized to give optimized geometries of **1H**$^{\bullet}$, **2H**$^{\bullet}$, and **3H**$^{\bullet}$. Selected bond lengths and angles for **3**$^{\bullet-}$, **3-azo**$^{\bullet-}$, and **3H**$^{\bullet}$ are listed in Table 1; values for all the reduced species are listed in Table S4. The optimized geometry of **3**$^{\bullet-}$ was calculated to be ca. 9.6 kJ mol^{-1} lower in energy than that of **3-azo**$^{\bullet-}$; the calculations suggest that the hydrazone is more stable than the azo tautomer in the radical, as both calculated and observed for the parent forms.

Both reduction and subsequent protonation give significant changes in the calculated geometries of the dyes. On going from **3** to **3**$^{\bullet-}$, the largest calculated change is the lengthening of the

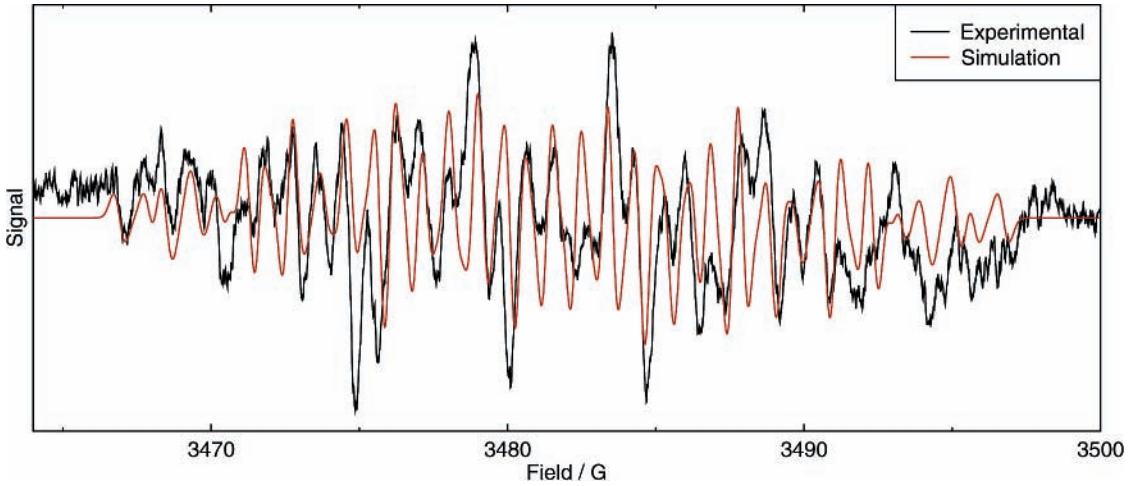

Figure 7. Experimental EPR spectrum of Orange II following reduction in aqueous solution at pH 4 (after subtraction of signals from other species observed in the absence of Orange II; see text). The simulated spectrum (see text and Table 6) was calculated using a modulation amplitude of 0.5 G and a line width of 0.4 G.

TABLE 5: Electron Spin Densities for Reduced Dye 3 Species Calculated at the B3LYP/6-31G(d) Level

	species		
atom	**3**$^{\bullet-}$	**3-azo**$^{\bullet-}$	**3H**$^{\bullet}$
N_1	0.386	0.350	0.434
N_{11}	0.022	0.126	0.151
C_1	−0.077	−0.130	−0.159
C_2	0.117	0.184	0.258
C_3	−0.021	−0.078	−0.131
C_4	0.157	0.218	0.269
C_{10}	0.098	0.103	0.116
O_2	0.164	0.056	0.038

N−N bond from 1.315 to 1.356 Å. Other notable changes are the shortening of the $C_{11}-N_{11}$ bond, the lengthening of the C_2-O_2 bond, and the lengthening of the N_1-C_1 bond; the bond lengths in the naphthyl ring are affected more than those in the phenyl ring. The same general trends on reduction are calculated for **1**, **2**, and **3-azo**; for example, on going from **3-azo** to **3-azo**$^{\bullet-}$, the N−N bond lengthens from 1.280 to 1.342 Å, which is longer than the nominally single N−N bond calculated for **3** (1.315 Å). Considering both reduction and subsequent protonation, the largest calculated differences on going from **3** to **3H**$^{\bullet}$ are the lengthening of the N−N bond from 1.315 to 1.337 Å, the lengthening of the C_2-O_2 bond, and the shortening of the C_1-C_2 bond; similar trends are calculated for **1** and **2** (Tables S1 and S4).

EPR Calculations. Mulliken electron spin densities and hyperfine splittings were calculated at the B3LYP/6-31G(d) level for the radical anions, **1**$^{\bullet-}$, **2**$^{\bullet-}$, **3**$^{\bullet-}$, and **3-azo**$^{\bullet-}$, and their protonated forms, **1H**$^{\bullet}$, **2H**$^{\bullet}$, and **3H**$^{\bullet}$. Additionally, splittings were calculated for **1**$^{\bullet-}$ and **1H**$^{\bullet}$ using the EPR-II basis set which is optimized for calculating EPR parameters: no EPR-II basis parameters are available for sulfur atoms, precluding such calculations on **2** and **3**. Table 5 lists the atoms which have the highest calculated spin densities (>0.10) for **3**$^{\bullet-}$, **3-azo**$^{\bullet-}$, and **3H**$^{\bullet}$; values calculated for all the dyes are listed in Table S5. In each case, the atom with the highest calculated spin density (ca. 0.40) is N_1, the nitrogen atom attached to the naphthyl ring, and there is significant spin density also on the carbon atoms C_1, C_2, C_4, and C_{10} within the naphthyl ring which is attached directly to this nitrogen atom. For **3**$^{\bullet-}$, the carbonyl oxygen atom O_2 also has significant calculated spin density (0.164). For **3-azo**$^{\bullet-}$ and **3H**$^{\bullet}$, not only N_1 but also N_{11} has a high calculated spin density (>0.10), and O_2 has a lower spin density (<0.10) than for **3**$^{\bullet-}$. The same atoms within the naphthyl ring have high calculated spin densities for **3**$^{\bullet-}$, **3-azo**$^{\bullet-}$, and **3H**$^{\bullet}$, but these spin densities are highest for **3H**$^{\bullet}$. Figure 8 shows the atoms within **3H**$^{\bullet}$ which have calculated spin densities of magnitude > 0.100. Nitrogens with a high spin density, and protons attached to atoms with a high spin density, may be expected to give rise to observable EPR splittings, but the nature of the relevant orbitals must be considered also to obtain their magnitudes.

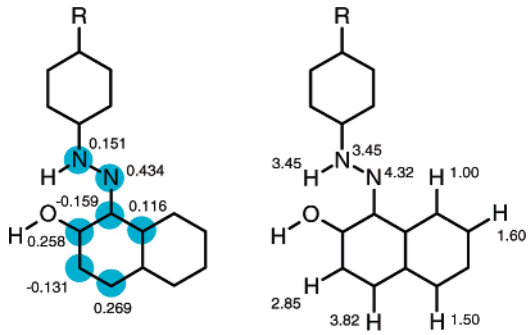

Figure 8. Left: (shaded circles) locations of high electron spin densities (>0.10) calculated for **3H**$^{\bullet}$ at the B3LYP/6-31G(d) level. Right: Proposed assignments of the hyperfine splittings (*G*) derived from the experimental EPR spectrum of reduced Orange II at pH 4 in aqueous solution.

Calculated hyperfine splittings for the reduced forms of **1** and **3** are listed in Table 6, with those for **2** listed in Table S6. The calculations on **3**$^{\bullet-}$ show a significantly larger splitting for N_1 than for N_{11}, whereas the relative splittings from the two nitrogens of **3H**$^{\bullet}$ are more similar, consistent with an increase in spin density at N_{11} on protonation (Table 5). The two large nitrogen splittings obtained from the simulation of the observed EPR spectrum support its assignment to the protonated radical anion of Orange II. All of the calculations give a higher splitting for N_1 than N_{11}, and, consequently, the two nitrogen splittings in the experimental EPR spectrum may be assigned to N_1 (4.32 G) and N_{11} (3.45 G). The magnitudes of the three highest calculated proton splittings of **1H**$^{\bullet}$ and **3H**$^{\bullet}$ are consistently in the order $H_4 > H_\alpha > H_3$, and, consequently, the three highest proton splittings from the experimental spectrum may be assigned tentatively in this order (Figure 8; Table 6). The remaining three proton splittings from the simulation are tentatively assigned in the order $H_8 > H_6 > H_9$, in agreement with their order in the EPR-II calculation and arising from protons in the other ring of the naphthyl group.

TABLE 6: Hyperfine Splittings (*G*) Calculated for Reduced Dye 1 and 3 Species and Assignments of Experimental Splittings of Reduced Orange II Radicals

	1$^{\bullet-}$		**3**$^{\bullet-}$	**3-azo**$^{\bullet-}$	**1H**$^{\bullet}$		**3H**$^{\bullet}$	Orange II H$^{\bullet}$
atom	EPR-II	6-31G(d)	6-31G(d)	6-31G(d)	EPR-II	6-31G(d)	6-31G(d)	experiment
N_1	6.13	8.39	7.50	6.61	6.76	8.15	8.39	4.32
N_{11}	0.25	1.12	−0.07	2.19	2.17	3.52	2.78	3.45
H_3	−0.51	−0.41	−0.33	1.08	2.58	2.47	2.27	2.85
H_4	−3.33	−3.69	−3.77	−5.24	−6.66	−6.70	−6.52	3.82
H_6	−0.58	−0.56	−0.42	−1.00	−2.12	−1.93	−1.50	1.50
H_7	0.14	0.22	−0.04	0.77	1.67	1.49	1.12	
H_8	−1.33	−1.31	−1.05	−1.30	−2.25	−2.07	−1.69	1.60
H_9	0.86	0.89	0.45	0.88	1.91	1.71	1.27	1.00
H_{12}	−0.98	−1.19	−0.86	−1.39	−1.39	−1.59	−1.62	
H_{13}	0.24	0.33	−0.11	−1.11	0.50	0.61	0.64	
H_{14}	−1.67	−1.96			−1.62	−1.87		
H_{15}	0.37	0.53	0.30	0.48	0.52	0.62	0.77	
H_{16}	−1.42	−1.75	−1.34	−2.09	−1.61	−1.86	−1.87	
H_α	−2.75	−3.06	−1.68		−5.92	−6.34	−5.51	3.45
H_β				−1.49	−1.28	−1.25	−1.27	

Vibrational Spectroscopy. Attempts were made to record resonance Raman spectra of the Orange II radical anion by using a photochemical reduction method comprising a UV initiating laser beam (363.8 nm) and three alternative visible probing laser beams (406.7, 568.2, or 647.1 nm) focused collinearly into a flowing solution of Orange II and an α-hydroxyketone photoreductant.[13] A small decrease in the intensities of the Orange II bands occurred when the UV beam was present, showing that dye reduction was occurring, but no new bands were observed. It is likely that the resonance Raman cross-sections of the reduced species are too low for bands to be observed under the conditions used (see Electronic Structure below). Although there are no experimental spectra for comparison, calculated IR and Raman spectra of **1**$^{\bullet-}$, **3**$^{\bullet-}$, **1H**$^{\bullet}$, and **3H**$^{\bullet}$ are provided here as Supporting Information (Figure S6) because they may assist in the assignment of radical spectra obtained by other methods (e.g. spectroelectrochemical or time-resolved).

Electronic Structure. Pulse radiolysis studies reported in the literature[39] have shown that reduction of Orange II in aqueous solution results in a difference spectrum with a strong bleach at ca. 490 nm and weak transient absorption at $\lambda > 550$ nm and $\lambda < 450$ nm, indicating that the reduced dye has lower peak absorption coefficients than the parent dye; these low absorption coefficients may explain the absence of resonance Raman bands from reduced species in our flow resonance Raman studies (see above). The lowest three electronic transitions of **3**$^{\bullet-}$ and **3H**$^{\bullet}$ were calculated by both the PBE1PBE/6-31G(d) TD-DFT and ZINDO semiempirical methods, and the calculated transition energies and oscillator strengths are tabulated in Table 4. The values calculated by the two methods are quite different from each other; the ab initio TD-DFT method may be expected to give better calculated properties for this open-shell system. The TD-DFT calculations on both **3**$^{\bullet-}$ and **3H**$^{\bullet}$ give a lowest energy transition which is lower in energy than that of **3** and **3-azo**, and which has a moderate oscillator strength that is much lower than that of the strongest parent transition (ca. 5%); this is consistent with the report of a weak radical band at longer wavelength than the strongest parent band.[39] The changes in electron density arising from the calculated transitions of **3**$^{\bullet-}$ and **3H**$^{\bullet}$ (Figure 6) are different from each other and from those of the parent dye. However, all are calculated to involve some transfer of electron density from the nitrogen atoms, particularly from N_{11}, to other parts of the molecule, and all except the lowest energy transition of **3H**$^{\bullet}$ involve electron transfer from O_2.

Implications for Reactivity. Reduction of Orange II with the 2-hydroxy-2-propyl radical, followed by rapid protonation of the radical anion, gives the short-lived Orange II hydrazyl radical detected here by EPR spectroscopy. Pulse radiolysis studies of Orange I and sodium 1-(phenylazo)-2-hydroxynaphthalene-6-sulfonate, which are both isomers of Orange II, have revealed that their hydrazyl radicals react by disproportionation at close to diffusion-controlled rates, with second-order rate constants of ca. 10^{10} dm^3 mol^{-1} s^{-1}.[42,43] The EPR spectrum of the Orange II hydrazyl radical reported here, along with calculations that give a high electron spin density at N_1, provide strong support for an intermolecular disproportionation mechanism in which a hydrogen atom transfer occurs from N_{11} to the nominal radical center at N_1 to give Orange II and its colorless hydrazide (Scheme 2). In reductive metabolism, the N−N bond of the hydrazide is subsequently cleaved to give aromatic amines.[5−9] The structure of the hydrazyl radical suggests that it may be able to undergo intermolecular hydrogen-atom abstraction reactions with other species and substrates, and not only by disproportionation with another radical; this general route to reductive dye degradation via the hydrazide may operate in a wider range of conditions than those studied here.

SCHEME 2: Disproportionation of Orange II Hydrazyl Radical

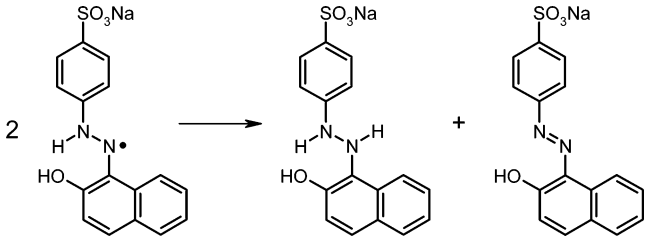

Conclusions

NMR, infrared, Raman, and UV−visible spectroscopy have been used to study the structure and bonding of Orange II in solution. NMR spectroscopy shows that Orange II is present predominantly as the hydrazone tautomer in aqueous solution and as a ca. 70:30 hydrazone:azo mixture in DMSO, in which the azo and hydrazone groups are internally hydrogen-bonded. The infrared and Raman spectra have been assigned with the assistance of DFT calculations, with many of the calculated modes involving contributions from several parts of the molecule. The intense absorption band of the hydrazone form of Orange II may be attributed to a charge-transfer transition involving the hydrazone group and the naphthyl ring; the intense absorption band of the azo form of Orange II may be attributed

to a charge-transfer transition from the naphthyl ring onto the two nitrogen atoms in the azo group.

Reduction of Orange II gives a hydrazyl radical which has been detected by EPR spectroscopy and which has significant electron spin density on the nitrogen atoms and the naphthyl ring. DFT calculations have aided the assignment of the experimental EPR spectrum, and they have also indicated the key changes in structure and bonding that occur on formation of the radical: a high electron spin density at one of the nitrogen atoms is proposed to promote the reported disproportionation reaction that leads to degradation of the dye.

Acknowledgment. We thank Ms. Heather Fish for recording NMR spectra, and the White Rose Consortium for providing the computing facilities that enabled the TD-DFT calculations. We acknowledge the support of Unilever Research.

Supporting Information Available: Tables and Figures giving additional results from DFT calculations (pdf). This material is available free of charge via the Internet at http://pubs.acs.org.

References and Notes

(1) Zollinger, H. *Color Chemistry*, 3rd ed.; Wiley-VCH: Weinheim, Germany, 2003.
(2) Oakes, J.; Gratton, P. *J. Chem. Soc., Perkin Trans. 2* **1998**, 1857.
(3) Oakes, J.; Gratton, P.; Clark, R.; Wilkes, I. *J. Chem. Soc., Perkin Trans. 2* **1998**, 2569.
(4) Oakes, J.; Gratton, P. *J. Chem. Soc., Perkin Trans. 2* **1998**, 2563.
(5) Glezer, V. In *The Chemistry of the Hydrazo, Azo and Azoxy Groups*; Patai, S., Ed.; Wiley: New York, 1997; p 729.
(6) Ozyurt M.; Atacag H. *Fresenius Environ. Bull.* **2003**, *12*, 1294.
(7) dos Santos, A. B.; Cervantes, F. J.; van Lier J. B. *Appl. Microbiol. Biotechnol.* **2004**, 64, 62.
(8) Sponza D. T.; Isik M. *Enzyme Microb. Technol.* **2004**, *34*, 147.
(9) Rao, P. S.; Hayon, E. *J. Phys. Chem.* **1973**, *77*, 2753.
(10) Hon, D. N.-S. *J. Polym. Sci., Polym. Chem. Ed.* **1979**, *17*, 441.
(11) Sirbiladze, K. J.; Rusznak, I.; Vig, A.; Krichevskiy, G. E.; Anyisimova, O. M.; Anyisimov, V. M. *Dyes Pigm.* **1992**, *19*, 235.
(12) Rémi, E.; Horváth, O.; Víg, A.; Rockenbauer, A.; Korecz, L.; Aranyosi, P.; Rusznák, I. *Radiat. Phys. Chem.* **1996**, *47*, 461.
(13) (a) Hunt, P.; Worrall, D. R.; Wilkinson, F.; Batchelor, S. N. *J. Am. Chem. Soc.* **2002**, *124*, 8532. (b) Batchelor, S. N. *New J. Chem.* **2004**, *28*, 1200.
(14) Olivieri, A. C.; Wilson, R. B.; Paul, I. C.; Curtin, D. Y. *J. Am. Chem. Soc.* **1989**, *111*, 5525.
(15) Ojala, W. H.; Lu, L. K.; Albers, K. E.; Gleason, W. B. *Acta Crystallogr.* **1994**, *B50*, 684.
(16) Ojala, W. H.; Sudbeck, E. A.; Lu, L. K.; Richardson, T. I.; Lovrien, R. E.; Gleason, W. B. *J. Am. Chem. Soc.* **1996**, *118*, 2131.
(17) (a) Kennedy, A. R.; McNair, C.; Smith, W. E.; Chisholm, G.; Teat, S. J. *Angew. Chem., Int. Ed.* **2000**, *39*, 638. (b) Kennedy, A. R.; Hughes, M. P.; Monaghan, M. L.; Staunton, E.; Teat, S. J.; Smith, W. E. *J. Chem. Soc., Dalton Trans.* **2001**, 2199. (c) Kennedy, A. R.; Kirkhouse, J. B. A.; McCarney, K. M.; Puissegur, O.; Smith, E. W.; Staunton, E.; Teat, S. J.; Cherryman, J. C.; James, R. *Chem. Eur. J.* **2004**, *10*, 4606.
(18) Park, K.-M.; Yoon, I.; Lee, S. S.; Choi, G.; Lee, J. S. *Dyes Pigm.* **2002**, *54*, 155.
(19) Malone, J. F.; Andrews, S. J.; Bullock, J. F.; Docherty, R. *Dyes Pigm.* **1996**, *30*, 183.
(20) Abbott, L. C.; Batchelor, S. N.; Jansen, L.; Oakes, J.; Lindsay Smith, J. R.; Moore, J. N. *New J. Chem.* **2004**, *28*, 815.
(21) Lyčka, A. *Ann. Rep. NMR Spectrosc.* **1993**, *26*, 247.
(22) Szántay, C., Jr.; Csepregi, Z.; Aranyosi, P.; Rusznák, I.; Töke, L.; Víg, A. *Magn. Reson. Chem.* **1997**, *35*, 306.
(23) (a) Murakami, K. *Dyes Pigm.* **2002**, *53*, 31. (b) Wang, J. C. *Adv. Colour Sci. Technol.* **2000**, *3*, 20.
(24) Reeves, R. L.; Maggio. M. S.; Harkaway, S. A. *J. Phys. Chem.* **1979**, *83*, 2359.
(25) Cross, W. I.; Flower, K. R.; Pritchard, R. G. *J. Chem. Res., Synop.* **1999**, 178.
(26) Asakura, T.; Ishida, M. *J. Colloid Interface Sci.* **1989**, *130*, 184.
(27) Armstrong, D. R.; Clarkson, J.; Smith, W. E. *J. Phys. Chem.* **1995**, *99*, 17825.
(28) Clarkson, J.; Armstrong, D. R.; Munro, C. H.; Smith, W. E. *J. Raman Spectrosc.* **1998**, *29*, 421.
(29) Littleford, R. E. Hughes, M. P.; Dent, G. Tackley, D.; Smith, W. E. *Appl. Spectrosc.* **2003**, *57*, 977.
(30) Biswas, N.; Umapathy, S. *J. Phys. Chem. A* **2000**, *104*, 2734.
(31) Dines, T. J.; Onoh, H. *J. Raman Spectrosc.* **2004**, *35*, 284.
(32) Dines, T. J.; MacGregor, L. D.; Rochester, C. H. *Phys. Chem. Chem. Phys.* **2004**, 4096.
(33) Dines, T. J.; Wu, H. *J. Phys. Chem. B* **2004**, *108*, 13456.
(34) Abbott, L. C.; Batchelor, S. N.; Oakes, J.; Lindsay Smith, J. R.; Moore, J. N. *J. Phys. Chem. A* **2004**, *108*, 10208.
(35) Åstrand, P.-O.; Ramanujam, P. S.; Hvilsted, S.; Bak, K. L.; Sauer, S. P. A. *J. Am. Chem. Soc.* **2000**, *122*, 3482.
(36) Guillaumont, D.; Nakamura, S. *Dyes Pigm.* **2000**, *46*, 85.
(37) Tackley, D. R.; Dent, G.; Smith, W. E. *Phys. Chem. Chem. Phys.* **2000**, *2*, 3949.
(38) Tackley, D. R.; Dent, G.; Smith, W. E. *Phys. Chem. Chem. Phys.* **2001**, *3*, 1419.
(39) Vinodgopal, K.; Kamat, P. V. *J. Photochem. Photobiol., A* **1994**, *83*, 141.
(40) Nasr, C.; Vinodgopal, K.; Hotchandani, S.; Chattopadhyay, A. K.; Kamat, P. V. *Radiat. Phys. Chem.* **1997**, *49*, 159.
(41) Neevel, J. G.; van Beek, H. C. A.; van de Graaf, B. *J. Soc. Dyers Colour.* **1992**, *108*, 150.
(42) Sharma, K. K.; O'Neill, P.; Oakes, J.; Batchelor, S. N.; Rao, B. S. M. *J. Phys. Chem. A* **2003**, *107*, 7619.
(43) Sharma, K. K.; Rao, B. S. M.; Mohan, H.; Mittal, J. P.; Oakes, J.; O'Neill, P. *J. Phys. Chem. A* **2002**, *106*, 2915.
(44) Zielonka, J.; Podsiadly, R.; Czerwińska, M.; Sikora, A.; Sokolowska, J.; Marcinek, A. *J. Photochem. Photobiol., A* **2004**, *163*, 373.
(45) Neta, P.; Levanon, H. *J. Phys. Chem.* **1977**, *81*, 2288.
(46) Flamigni, L.; Monti, S. *J. Phys. Chem.* **1985**, *89*, 3702.
(47) Monti, S.; Flamigni, L. *J. Phys. Chem.* **1986**, *90*, 1179.
(48) Krapfenbauer, K.; Wolfger, H.; Getoff, N.; Hamblett, I.; Navaratnam, S. *Radiat. Phys. Chem.* **2000**, *58*, 21.
(49) Das, S.; Kamat, P. V.; Padmaja, S.; Au, V.; Madison, S. A. *J. Chem. Soc., Perkin Trans. 2* **1999**, 1219.
(50) Heijkoop, G.; van Beek, H. C. A. *Recl. Trav. Chim. Pays-Bas* **1977**, *96*, 83.
(51) Duling, D. R. *J. Magn. Reson.* **1994**, *B104*, 105.
(52) Dixon, W. T.; Norman, R. O. C. *J. Chem. Soc.* **1963**, 3119.
(53) Gilbert, B. C.; Jeff, M. In *Free Radicals: Chemistry, Pathology, and Medicine*; Rice-Evans, C., Dormandy, T., Eds.; Richelieu Press: London; 1988; pp 25−49.
(54) Norman, R. O. C.; Gilbert, B. C. *Adv. Phys. Org. Chem.* **1967**, *5*, 53.
(55) Frisch, M. J.; Trucks, G. W.; Schlegel, H. B.; Scuseria, G. E.; Robb, M. A.; Cheeseman, J. R.; Zakrzewski, V. G.; Montgomery, J. A., Jr.; Stratmann, R. E.; Burant, J. C.; Dapprich, S.; Millam, J. M.; Daniels, A. D.; Kudin, K. N.; Strain, M. C.; Farkas, O.; Tomasi, J.; Barone, V.; Cossi, M.; Cammi, R.; Mennucci, B.; Pomelli, C.; Adamo, C.; Clifford, S.; Ochterski, J.; Petersson, G. A.; Ayala, P. Y.; Cui, Q.; Morokuma, K.; Malick, D. K.; Rabuck, A. D.; Raghavachari, K.; Foresman, J. B.; Cioslowski, J.; Ortiz, J. V.; Baboul, A. G.; Stefanov, B. B.; Liu, G.; Liashenko, A.; Piskorz, P.; Komaromi, I.; Gomperts, R.; Martin, R. L.; Fox, D. J.; Keith, T.; Al-Laham, M. A.; Peng, C. Y.; Nanayakkara, A.; Gonzalez, C.; Challacombe, M.; Gill, P. M. W.; Johnson, B. G.; Chen, W.; Wong, M. W.; Andres, J. L.; Gonzalez, C.; Head-Gordon, M.; Replogle, E. S.; Pople, J. A. *Gaussian 98*, Revision A.7; Gaussian, Inc.: Pittsburgh, PA, 1998.
(56) Frisch, M. J.; Trucks, G. W.; Schlegel, H. B.; Scuseria, G. E.; Robb, M. A.; Cheeseman, J. R.; Montgomery, J. A., Jr.; Vreven, T.; Kudin, K. N.; Burant, J. C.; Millam, J. M.; Iyengar, S. S.; Tomasi, J.; Barone, V.; Mennucci, B.; Cossi, M.; Scalmani, G.; Rega, N.; Petersson, G. A.; Nakatsuji, H.; Hada, M.; Ehara, M.; Toyota, K.; Fukuda, R.; Hasegawa, J.; Ishida, M.; Nakajima, T.; Honda, Y.; Kitao, O.; Nakai, H.; Klene, M.; Li, X.; Knox, J. E.; Hratchian, H. P.; Cross, J. B.; Adamo, C.; Jaramillo, J.; Gomperts, R.; Stratmann, R. E.; Yazyev, O.; Austin, A. J.; Cammi, R.; Pomelli, C.; Ochterski, J. W.; Ayala, P. Y.; Morokuma, K.; Voth, G. A.; Salvador, P.; Dannenberg, J. J.; Zakrzewski, V. G.; Dapprich, S.; Daniels, A. D.; Strain, M. C.; Farkas, O.; Malick, D. K.; Rabuck, A. D.; Raghavachari, K.; Foresman, J. B.; Ortiz, J. V.; Cui, Q.; Baboul, A. G.; Clifford, S.; Cioslowski, J.; Stefanov, B. B.; Liu, G.; Liashenko, A.; Piskorz, P.; Komaromi, I.; Martin, R. L.; Fox, D. J.; Keith, T.; Al-Laham, M. A.; Peng, C. Y.; Nanayakkara, A.; Challacombe, M.; Gill, P. M. W.; Johnson, B. G.; Chen, W.; Wong, M. W.; Gonzalez, C.; Pople, J. A. *Gaussian 03*, Revision B.05; Gaussian, Inc.: Pittsburgh, PA, 2003.
(57) Mayo, S. L.; Olafson, B. D.; Goddard, W. A. *J. Phys. Chem.* **1990**, *94*, 8897.
(58) (a) Becke, A. D. *J. Chem. Phys.* **1993**, *98*, 5648. (b) Lee, C.; Yang, W.; Parr, R. G. *Phys. Rev. B* **1988**, *37*, 785.
(59) Wolinski, K.; Hilton, J. F.; Pulay, P. *J. Am. Chem. Soc.* **1990**, *112*, 8251.
(60) Scott, A. P.; Radom, L. *J. Phys. Chem.* **1996**, *100*, 16502.
(61) (a) Anderson, W. P.; Edwards, W. D.; Zerner, M. C. *Inorg. Chem.* **1986**, *25*, 2728. (b) Ridley, J.; Zerner, M. C. *Theor. Chim. Acta* **1973**, *32*,

111. (c) Edwards, W. D.; Ohrn, N. Y.; Weiner, B. L.; Zerner, M. C. *Int. J. Quantum Chem., Quantum Chem. Symp.* **1984**, *18*, 507.

(62) (a) Perdew, J. P.; Burke, K.; Ernzerhof, M. *Phys. Rev. Lett.* **1996**, *77*, 3865. (b) Adamo, C.; Barone, V. *J. Chem. Phys.* **1999**, *110*, 6158.

(63) Barone, V. In *Recent Advances in Density Functional Methods*, Part I; Chong, D. P., Ed.; World Scientific: Singapore, 1996.

(64) (a) Portmann, S.; Lüthi, H. P. *Chimia* **2000**, *54*, 766. (b) *Molekel*, www.cscs.ch/molekel.

(65) Schaftenaar, G.; Noordik, J. H. *J. Comput.-Aided Mol. Des.* **2000**, *14*, 123.

(66) Abbott, L. C.; Batchelor, S. N.; Oakes, J.; Lindsay Smith, J. R.; Moore, J. N. *J. Phys. Chem. B* **2004**, *108*, 13726.

(67) Bauer, C.; Jacques, P.; Kalt, A. *Chem. Phys. Lett.* **1999**, *307*, 397.

(68) Barnes, A. J.; Majid, M. A.; Stuckey, M. A.; Gregory, P.; Stead, C. V. *Spectrochim. Acta* **1985**, *41A*, 629.

(69) Reeves, R. L.; Kaiser, R. S. *J. Org. Chem.* **1970**, *35*, 3670.

(70) Fliegl, H.; Köhn, A.; Hättig, C.; Ahlrichs, R. *J. Am. Chem. Soc.* **2003**, *125*, 9821.

(71) Åstrand, P.-O.; Ramanujam, P. S.; Hvilsted, S.; Bak, K. L.; Sauer, S. P. A. *J. Am. Chem. Soc.* **2000**, *122*, 3482.

(72) Rau, H. In *Photochemistry and Photophysics*; Rabek, J. F., Ed.; CRC Press: Boca Raton, FL, 1990; Vol. II, pp 119−141.

(73) The relative concentrations in our experiments were [propan-2-ol]/[dye] = 1000/1. The literature rate constants for reaction of •OH with propan-2-ol[74] and a similar dye (Orange I)[42] are ca. 2×10^9 and ca. 1×10^{10} dm^3 mol^{-1} s^{-1}, respectively. Hence, the relative yield for reaction of •OH with propan-2-ol/dye is estimated as ca. 200/1, and direct reaction of •OH with the dye is negligible.

(74) Buxton, G. V.; Greenstock, C. L.; Helman, W. P.; Ross, A. B. *J. Phys. Chem. Ref. Data* **1988**, *17*, 513.

(75) Statško, A.; Erentová, K.; Rapta, P.; Nuyen, O.; Voit, B. *Magn. Reson. Chem.* **1998**, *36*, 13.

(76) Russell, G. A.; Konaka, R.; Strom, T.; Danen, W. C.; Chang, K.-Y.; Kaupp, G. *J. Am. Chem. Soc.* **1968**, *90*, 4646.

(77) Geels, E. J.; Konka, R.; Russell, A. *J. Chem. Soc., Chem. Commun.* **1965**, 13.

(78) Neugebauer, F. A.; Weger, H. *Chem. Ber.* **1975**, *108*, 2703.